Stagnation Points as Loci of Solute Concentration Extrema at the Evaporative Surface of a Random Porous Medium

Faiza Hidri, Babacar Diouf, R. Bouhlila, Sandrine Geoffroy, Marc Prat

HAL Id: hal-02278716
https://hal.insa-toulouse.fr/hal-02278716

Submitted on 13 Nov 2019

Stagnation Points as Loci of Solute Concentration Extrema at the Evaporative Surface of a Random Porous Medium

F. Hidri[1,2] · **B. Diouf**[3] · **R. Bouhlila**[2] · **S. Geoffroy**[3] · **M. Prat**[1]

Abstract Evaporation of a saline solution from a porous medium often leads to the precipitation of salt at the surface of the porous medium. It is commonly observed that the crystallized salt does not form everywhere at the porous medium surface but at some specific locations. This is interpreted at the signature of spatial variations in the salt concentration at the surface of the porous medium prior to the onset of crystallization. We explore numer-ically the link between the ion concentration spatial variations at the surface and porous medium heterogeneities considering strongly anisotropic short-range correlated permeabil-ity Gaussian fields corresponding to a vertical layering perpendicular to the top evaporative surface for the case of the evaporation–wicking situation. It is shown that the ion concentra-tion extrema at the surfaces correspond to stagnation points with minima corresponding to divergent stagnation points and maxima to convergent stagnation points. Counter-intuitively, the ion concentration maxima are shown to correspond to permeability minima. However, the ion concentration absolute maximum does not necessarily always correspond to the per-meability absolute minimum. More generally, the study emphasizes the key role played by the impact of heterogeneities on the velocity field induced in the medium by the evaporation process. It is also shown that the number of ion mass fraction maxima at the porous medium surface is generally much lower than the naive prediction based on the number of correlation lengths spanning the medium.

Keywords Evaporation · Solute transport · Saline solution · Stagnation points · Random porous medium

✉ M. Prat
mprat@imft.fr

[1] Institut de Mécanique des Fluides de Toulouse (IMFT), Université de Toulouse, CNRS, Toulouse, France

[2] Laboratoire de Modélisation en Hydraulique et Environnement, Ecole Nationale d'ingénieurs de Tunis, Université Tunis El Manar, BP 37, 1002 Tunis, Tunisia

[3] LMDC (Laboratoire Matériaux et Durabilité des Constructions), Université de Toulouse, INSAT, UPS, Toulouse, France

1 Introduction

Transport of a solute in a saturated porous medium is a classical problem which has motivated many studies over more than one century (e.g. Bear 1972; Dagan 1989; Fried and Combarnous 1971; Slichter 1905), and is still a very active research topic (e.g. Dentz et al. 2011; Le Borgne et al. 2013). Evaporation of water from porous media is also a topic of interest in relation to many aspects of water management, global water cycle, soil and groundwater salinization, agriculture, and other environmental issues. The topic has stimulated a significant amount of work (e.g. Brutsaert 2005; Or et al. 2013; Penman 1948) and references therein. Then, we have situations combining both evaporation from a porous medium and the transport of a solute. This type of situations is notably encountered when a porous medium containing a salty solution is exposed on one or several sides to air. Generally, this leads to the accumulation of ions in the regions adjacent to the evaporative surfaces of the porous medium (e.g. Guglielmini et al. 2008; Huinink et al. 2002; Puyate and Lawrence 1999, 2000; Puyate et al. 1998). As illustrated in previous works (e.g. Desarnaud et al. 2015; Hidri et al. 2013), the process can lead to the formation of salt crystals at the surface if the conditions are such that the ion concentration reaches the critical concentration marking the onset of crystallization. An issue in this context is to predict the most likely place of crystal formation at the porous medium surface. Two main factors have a clear impact on the loci of the first crystals at the surface. As shown in Veran-Tissoires et al. (2012a) and Veran-Tissoires and Prat (2014), the evaporation flux is a major factor. Crystals preferentially form where the evaporation flux is greater at the surface. This is so because the velocity induced in the porous medium is greater in the region where the evaporation flux is higher. The second factor is the heterogeneity of the medium. As shown and discussed, for example, in Diouf et al. (2018) and Veran-Tissoires et al. (2012b) for simple systems formed by the assembly of two vertical porous layers having different permeabilities, crystals start forming either at the surface of the fine medium or at the surface of the coarse medium depending on the conditions but not at the surface of both media. As discussed in some details in Diouf et al. (2018), the locus of first crystals on either the surface of the fine or the coarse porous medium depends on the evaporation configuration. When the system remains saturated by the solution because there is a permanent supply of solution at the system bottom, a situation referred to as the evaporation–wicking situation, crystals preferentially form at the surface of the fine medium. In the case of drying where the system is bounded by the top surface open to the ambient air and solid surfaces elsewhere, crystals preferentially form at the surface of the coarse medium, except when the initial salt concentration is close to solubility. (Then the situation is similar to the evaporation–wicking situation since the desaturation of the system is weak when the critical concentration is reached at the surface.) While the consideration of simple systems formed by the assembly of two vertical porous layers of different textures is instructive and has been considered in several previous works (Diouf et al. 2018; Veran-Tissoires et al. 2012b; Bechtold et al. 2011; Mejri et al. 2017; Nachshon et al. 2011a, b; Bergstad et al. 2017), heterogeneous porous media are generally less simple (e.g. Dagan 1989; Gelhar 1993). Therefore, there is a need for the study of more complex heterogeneous systems. In the present paper, we consider a random heterogeneous porous medium and concentrate on the evaporation–wicking situation, i.e. the situation where the medium is exposed on the bottom to a salty aqueous solution and on the other side to a sufficiently dry air for evaporation to occur on the top surface (e.g. Puyate and Lawrence 1999, 2000; Puyate et al. 1998). Assuming negligible porosity variations, we consider highly anisotropic random permeability fields where the permeability is spatially uniform along vertical lines and thus only varies in the horizontal direction. This can be

viewed as an extension of the previous works on vertically textured media formed by only two columns. We concentrate on the salt concentration distribution at the surface prior to any significant development of efflorescence. Since the focus is on the effect of heterogeneities, the evaporation flux is supposed spatially uniform over the top surface of the medium. The objective is to study the loci of the ion concentration extrema at the surface and in particular the loci of the ion concentration maxima since they correspond to the loci of incipient crystals when the maximum concentration reaches the critical salt concentration. The study is based on the numerical computation on the ion concentration field in the system.

The paper is organized as follows: The basic evaporation situation considered, namely the evaporation–wicking situation, is briefly described in Sect. 2. The type of heterogeneities and the method used to generate them are presented in Sect. 3. The problem formulation is presented in Sect. 4. The impact of heterogeneities on the velocity field, which is a key aspect in this problem, is discussed in Sect. 5. Section 6 presents the results on the ion distribution at the surface. Conclusions are drawn in Sect. 7.

2 The Evaporation–Wicking Situation

As sketched in Fig. 1, the sample is in contact at its bottom with an aqueous solution. The liquid is drawn into the pores by capillary suction. There is a permanent supply of solution, and therefore, a steady state is reached when the flow rate of liquid sucked into the medium by capillary action exactly balances the evaporation rate. The medium can be fully saturated by the solution when the capillary action is sufficiently strong or an internal evaporation front can exist when the capillary action is not sufficient to maintain the medium fully saturated. In this paper, the situation with a stabilized internal evaporation front is not considered. The medium is therefore assumed fully saturated by the solution.

A two-dimensional Cartesian square domain of size $L_x = L_y = L$ is considered. The size L of the domain is 0.1 m for all the simulations presented in this study. As porous materials, we consider more or less explicitly random packings of particles. This means that the parameters involved in the models will be computed using classical relationships developed for packings of particles.

3 Heterogeneities Generation

The method used for generating a two-dimensional short-range correlated Gaussian random field $h(x, y)$ is the same as the one described in Plouraboué et al. (2006). We focus on the impact of permeability disorder. This corresponds to random permeability fields with a constant porosity field ($\varepsilon = 0.375$). This is a good approximation, for example, for systems of particles where the porosity varies little with the particle diameter, whereas the permeability scales as the square of the particle diameter. For generating a random permeability field, we generate grain diameters d in the range $[d_{min}, d_{max}]$ with $d(x, y) = d_{min} + \left(\frac{h(x, y) - h_{min}}{h_{max} - h_{min}} \right) (d_{max} - d_{min})$, with $d_{min} = 10^{-5}$ m and $d_{max} = 10^{-4}$ m. Then, the local permeability k is computed using the Carman–Kozeny relationship $k = \frac{\varepsilon^3 d^2}{180(1-\varepsilon)^2}$ with a constant porosity equal to 0.375. This yields a permeability varying randomly (with x only) between 7.5×10^{-14} m^2 and 7.5×10^{-12} m^2.
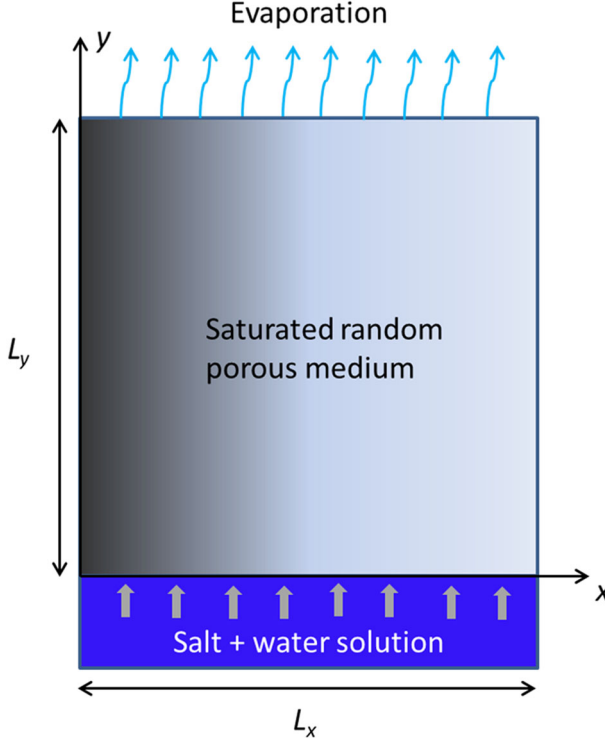
Fig. 1 Schematic of the evaporation–wicking situation

The random field h is generated using an anisotropic Gaussian correlation function of the form $C(\delta) = \exp\left[-\left(\frac{\delta_x}{l_{cx}}\right)^2 - \left(\frac{\delta_y}{l_{cy}}\right)^2\right]$ where l_{cx} and l_{cy} are the correlation lengths in the x and y directions, respectively. To obtain vertical layering, we simply take $l_{cx} \leq L$ and $l_{cy} > L$. In the present effort, only one value of correlation length is considered, namely $l_{cx}/L = 1/12$, $l_{cy} > L$ (vertical layering). Thus, the size of the computational domain is 12 correlation lengths. Thus, to construct our system, we have considered beads whose maximum diameter is 10^{-4} m. The computational domain size is 0.1 m, and the correlation length is 8.3 mm. As a result, there are about 80 beads over a correlation length (actually more since we consider here the maximum diameter). One can consider that a representative elementary volume (REV) of 8–10 bead diameters is sufficient for defining a local permeability. Thus, we have approximately 10 REV over the correlation length, which sounds sufficient to satisfy the criteria of length-scale separation underlying the continuum approach to porous media.

To further discuss the choice of the correlation length, we introduce the length scale $l_D = D_s^*/U_0$, where D_s^* is the effective diffusion coefficient of the ions and U_0 is a reference interstitial velocity, defined in what follows as $j/(\varepsilon\rho_\ell)$, where j is the evaporation flux at the surface, ε the porous medium porosity and ρ_ℓ the solution density. The length l_D can be interpreted as the length over which the diffusion averages out the velocity fluctuations. Introducing also the Peclet number, $Pe = \frac{U_0 L}{D_s^*}$, a key parameter in this type of problem (i.e. Guglielmini et al. 2008; Huinink et al. 2002), it can be seen that $l_D = L/Pe$. In the simulations presented in what follows, $Pe \sim [6\text{–}24]$ unless otherwise mentioned. Thus, $\frac{l_D}{L} \sim [1/6 - 1/24]$,
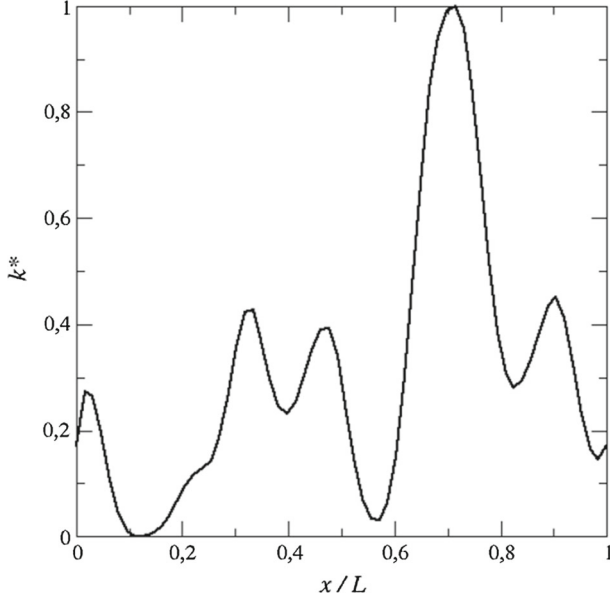
Fig. 2 Reference permeability disorder considered in the study; $k*$ is the reduced permeability: $k* = \frac{k - k_{\min}}{k_{\max} - k_{\min}}$

while $l_{cx}/L = 1/12$. Thus, we will mainly consider the regime where l_D is of the same order of magnitude as the correlation length. For much smaller correlation lengths, it can be expected that diffusion will average out the velocity fluctuations and thus that the spatial fluctuations of the ion concentration at the surface will be much smaller than studied in the present work.

Up to 10 realizations of the permeability random field will be considered. The one depicted in Fig. 2 is referred to as the reference case and will be discussed in more details.

4 Problem Formulation

Within the framework of the classical continuum approach to porous media, the equation governing the ion transport in the porous medium reads,

$$\frac{\partial \rho_\ell \varepsilon C}{\partial t} + \nabla \cdot (\rho_\ell \mathbf{V} C) = \nabla \cdot \left(\rho_\ell \varepsilon D_s^* \nabla C \right) \tag{1}$$

in which C is the mass fraction of dissolved salt, ρ_ℓ is the solution density, D_s^* is the effective diffusive coefficient of the dissolved salt in the liquid, $D_s^* = \varepsilon^{0.4} D_s$ (e.g. Kim et al. 1987), where D_s is the ion diffusion coefficient in water ($D_s \approx 1.3 \times 10^{-9}$ m^2/s). Note that the pore-scale Peclet number (constructed using a pore or grain length scale, i.e. $Pe_p = \frac{U_0 d}{D_s^*}$) is small under typical evaporation conditions. In the case of our simulations, $Pe_p = \frac{U_0 d}{D_s^*} \sim$ O$\left(10^{-4} - 10^{-3}\right)$. As a result, mechanical dispersion effects (e.g. Fried and Combarnous 1971) are ignored. The boundary conditions can be expressed as

$$C = C_0 \text{ at } y = 0. \tag{2}$$

$$(\rho_\ell \mathbf{V} C - \rho_\ell \varepsilon D_s^* \nabla C) \cdot \mathbf{n} = 0 \text{ at } y = L \; \forall x \text{ and at } x = 0 \text{ and } x = L \; \forall y > 0 \tag{3}$$

The zero flux boundary condition (3), where **n** is the unit vector normal to the considered surface, expresses that the dissolved salt cannot leave the porous medium before the onset of crystallization. The initial salt mass fraction in the porous domain is uniform and equal to C_0, i.e. $C = C_i = C_0$, throughout the sample at $t = 0$. To solve the above problem, the velocity field in the porous medium must be known. Using Darcy's law, the boundary value problem describing the flow in the porous medium is given by (after decomposition of the pressure according to $P = P_{vis} - \rho_\ell g y$),

$$\nabla \cdot \mathbf{V} = 0 \tag{4}$$

$$\mathbf{V} = -\frac{k}{\mu} \nabla P_{vis} \tag{5}$$

where μ is the liquid solution viscosity. Equations (4, 5) are solved subject to the following boundary conditions: $P_{vis} = P_0$ (arbitrary constant) at $y = 0$, $\mathbf{V} \cdot \mathbf{n} = 0$ on the porous domain lateral side. At the porous medium top surface, the evaporation flux j is balanced by the liquid flow coming from the porous medium,

$$\rho_\ell V_y = j \text{ at } y = L \tag{6}$$

where j is assumed to be constant and uniform over the surface. Defining the evaporation velocity as $V_0 = j/\rho_\ell$, Eq. (6) can be expressed as $V_y = V_0$ at $y = L$. We introduce a reference value for the evaporation velocity $V_{0ref} = 2 \times 10^{-8}$ m/s (thus on the order of 0.1 cm/day, a typical value for slow evaporation, e.g. Veran-Tissoires and Prat 2014). This gives as reference Peclet number, $Pe = \frac{U_0 L}{D_s^*} = \frac{V_{0ref} L}{\varepsilon D_s^*} \sim 6$, while the value of the *Peclet* number constructed using the correlation length is 0.5. The latter value simply reflects the fact that l_D and l_{cx} are on the same order of magnitude as pointed out in Sect. 3.

Note that for simplicity the variations of solution density and viscosity with salt mass fraction are ignored throughout the paper. The above problem is solved numerically using the commercial simulation software COMSOL Multiphysics after varying the mesh until solutions independent of the meshing are obtained.

5 Velocity Field

The crucial effect of heterogeneities is to induce a heterogeneous velocity field and consequently a heterogeneous advective transport of the ions.

This is illustrated in Fig. 3, which shows the computed velocity field for the reference case. Note that the velocity field is independent of time with our assumptions (constant solution viscosity and density and constant evaporation flux).

As expected, the velocity is on average directed towards the evaporative (top) surface of porous medium. This explains why ions tend to accumulate at the surface. In the absence of permeability heterogeneities, the filtration velocity **V** is spatially uniform.

The variation with x of the reduced permeability, defined as $k^* = \frac{k - k_{min}}{k_{max} - k_{min}}$, is shown in Fig. 2 for the reference case, whereas the corresponding velocity field is shown in Fig. 3. As shown in Figs. 2 and 3, the higher the permeability, the higher the velocity is. This holds within the porous domain but not at the porous medium surface where the velocity y-component is strictly uniform according to Eq. (6). Note, however, that the velocity x-component at the surface is not uniform, and as a result the velocity vector is not uniform at the surface as illustrated in Fig. 3. The major point here is that the structure of the velocity field in the upper region of the sample is different from the structure further away inside the porous domain.
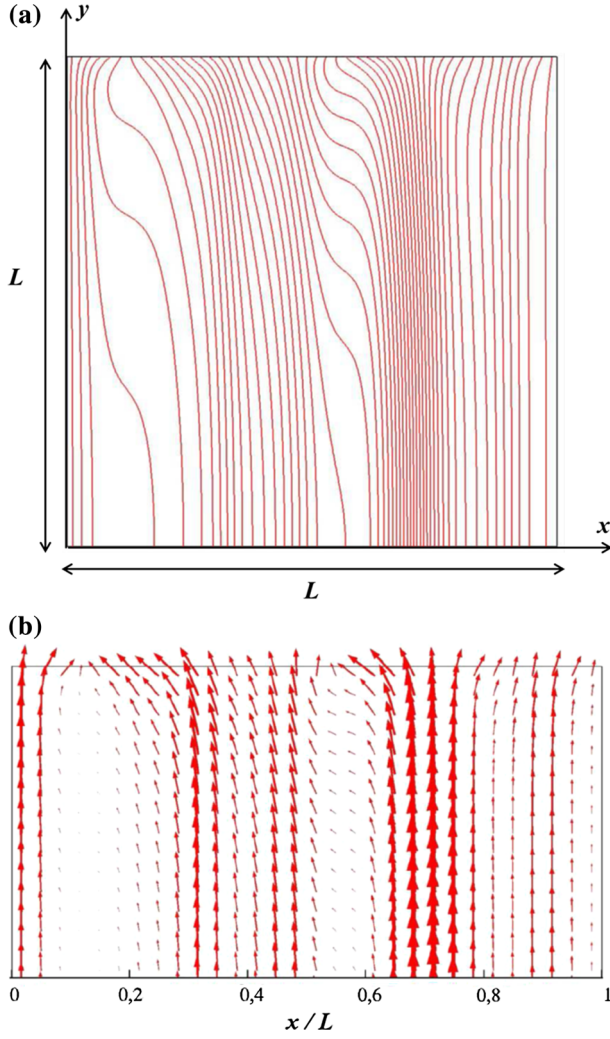
Fig. 3 Stream lines in the heterogeneous porous domain (**a**) and detailed view of velocity field in the top region (**b**) for the reference case

In particular, as illustrated in Fig. 3a, the velocity is non-uniform at the inlet of the porous domain. The velocity at the inlet varies as the permeability, thus is greater at the inlet of a region of greater permeability and lower at the inlet of a region of lower permeability. We can thus distinguish two main regions as regards the structure of the velocity field: the region sufficiently far away from the surface where the velocity field is essentially directed along the y direction and varies along the x direction and the region adjacent to the surface where the velocity y-component progressively becomes uniform. It is expected that the size of the near-surface region is on the order of the correlation length. This is illustrated in Fig. 4, which shows that the size of the region where the velocity variation changes sharply is about equal to two correlation lengths.
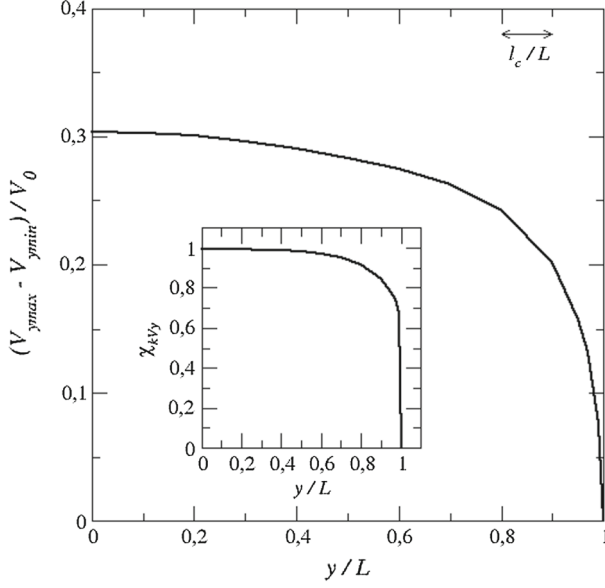
Fig. 4 Variation of $V_{y\max} - V_{y\min}$ as a function of y ($V_{y\max}(y) = \max(V_y(x, y)$ at y; $V_{y\min}(y) = \min(V_y(x, y)$ at y). The inset shows the variation of correlation coefficient between the permeability k and V_y

The pressure is actually almost independent of x near the inlet. As shown in "Appendix", one can use this feature to estimate the velocity distribution at the inlet. The result reads

$$V_y = \frac{k}{\langle k \rangle} V_{\text{ref}} \tag{7}$$

where $\langle k \rangle = \frac{1}{L_x} \int_0^{L_x} k \, dx$.

The prediction given by Eq. (7) is tested against the numerically computed velocity in Fig. 5. As can be seen, the agreement is quite good. Equation (7) clearly indicates that the flow is highly heterogeneous at the inlet.

Thus, from Eq. (7), it is expected that the velocity field is highly correlated to the permeability field far from the surface and progressively less and less correlated as the surface is approached. This is illustrated in the inset of Fig. 4, which shows the variation

of the correlation coefficient $\chi_{Vk}(y) = \dfrac{\int_0^L (V_y^* - \bar{V}_y^*)(k^* - \bar{k}^*) dx}{\int_0^L (V_y^* - \bar{V}_y^*)^2 dx \int_0^L (k^* - \bar{k}^*)^2 dx}$ as a function of y, where

$V_y^*(x, y) = \dfrac{V_y(x, y) - V_{y\min}(y)}{V_{y\max}(y) - V_{y\min}(y)}$. Using Eq. (7) in the expression of $\chi_{Vk}(0)$ obviously leads to $\chi_{Vk}(0) = 1$ in agreement with the computed value shown in the inset of Fig. 4.

A second major feature is that the velocity contrast in the region away from the near-surface region is quite high. Expressed in terms of local Peclet number $Pe(x) = \dfrac{V_y L}{\varepsilon D_s^*}$, the velocity contrast is characterized by a local Peclet number varying between 0.2 and 15 for the case corresponding to the reference evaporation velocity $V_{0\text{ref}}$. As mentioned before, the average Peclet number is defined as $Pe = \dfrac{V_0 L}{\varepsilon D_s^*}$. Thus, $Pe \approx 6$ for $V_0 = V_{0\text{ref}}$.
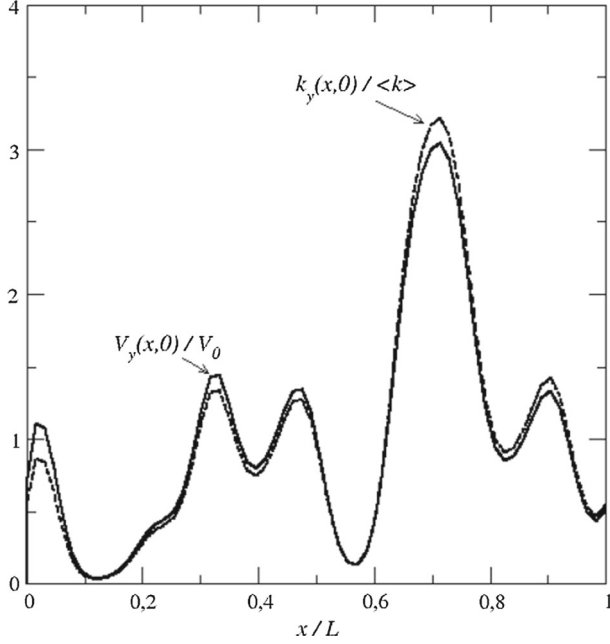
Fig. 5 Plot of V_y/V_0 and $\frac{k}{\langle k \rangle}$ at the inlet

6 Ion Distribution

The distribution of the ion mass fraction at the surface is studied in terms of the reduced ion mass fraction $C^*(t) = \frac{C(t)-C_{\min}(t)}{C_{\max}(t)-C_{\min}(t)}$ at porous medium surface, where $C_{\max}$ and $C_{\min}$ are the maximum and minimum ion mass fractions at time t at the porous medium surface. Based on the importance of advection transport in this problem, a naïve view is thus to infer that the ion mass fraction maxima must correspond to the permeability maxima since the permeability maxima correspond to region of higher velocities and thus to higher advection transport of the ions. As shown in Fig. 6 for the short-time regime (defined as the period when $W(t)/l_c \ll 1$ where $W(t)$ denotes the thickness of the peak region, i.e. the region adjacent to the surface where the ion mass fraction gradients are significant), this is exactly the contrary which is observed. The ion mass fraction distribution is anticorrelated with the permeability and thus reasonably well correlated with $1 - k^*$. We have also plotted in Fig. 6 the evolution of $1 - V_y^*$ at $y/L = 0.99$, i.e. close to the surface. As can be seen, the ion mass fraction distribution is still better correlated with $1 - V_y^*$ than with $1 - k^*$. This is not really surprising since (1) the velocity field is the key point in this problem, (2) the correlation between the permeability field and the velocity field ceases to be excellent and becomes even zero right at the surface in the near-surface region (as illustrated in the inset of Fig. 4). The strong correlation between C^* and $1 - V_y^*$ right below the surface depicted in Fig. 6 can be qualitatively explained as follows. We introduce the excess mass fraction $C_{ex} = C - C_0$. The problem governing C_{ex} in the short times is deduced from Eqs. (1–3) and read

$$\frac{\partial \rho_\ell \varepsilon C_{ex}}{\partial t} + \nabla \cdot (\rho_\ell \mathbf{V} C_{ex}) = \nabla \cdot \left(\rho_\ell \varepsilon D_s^* \nabla C_{ex} \right) \tag{8}$$
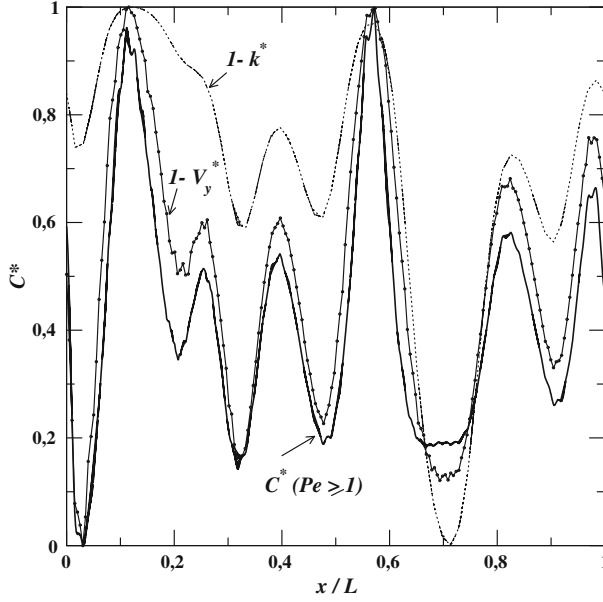
$$C_{ex} = 0 \text{ away from the top surface} \tag{9}$$

Fig. 6 Distribution of reduced ion mass fraction $C^* = (C(t)-C_{\min}(t))/(C_{\max}(t)-C_{\min}(t))$ at the porous medium surface for various Peclet numbers when $W(t)/l_c \ll 1$ (short-time regime, $t = 5$ h). The amplitude ratio $C_{\max}/C_{\min}$ is here only very slightly greater than 1, equal to 1.003 for $Pe = 40$ for example. $V_y^* = \left(V_y(t) - V_{y\min}(t)\right) / \left(V_{y\max}(t) - V_{y\min}(t)\right)$ at $y/L = 0.99$

$$(\rho_\ell \mathbf{V} C_{\mathrm{ex}} - \rho_\ell \varepsilon D_{\mathrm{s}}^* \nabla C_{\mathrm{ex}}) \cdot \mathbf{n} = 0 \text{ at } x = 0 \text{ and } x = L \; \forall y > 0 \tag{10}$$

$$\rho_\ell V_0 C_{\mathrm{ex}} - \rho_\ell \varepsilon D_{\mathrm{s}}^* \frac{\partial C_{\mathrm{ex}}}{\partial y} = -\rho_\ell V_0 C_0 \text{ at } y = L \; \forall x \tag{11}$$

This problem is analogous to a problem in which the ions in excess (accumulating in the top region) are injected with a uniform flux $-\rho_\ell V_0 C_0$ along the top surface. Then consider a small square control volume attached to a point at the surface. The mass transfer rate of ions in excess is zero through the bottom surface of the control volume (short-time regime) and the same everywhere through the top surface of the control volume since the excess ion flux $(= -\rho_\ell V_0 C_0)$ is uniform over the surface. Then consider the velocity component V_y below the surface, at $y/L = 0.99$ for example. Wherever $V_{y0.99} < V_0$, where V_0 is the velocity along the y direction everywhere at the surface, mass conservation implies that a net flow rate enters the control volume from the lateral sides, bringing additional ions in the control volume. On the contrary, where $V_{y0.99} > V_0$, a net flow rate leaves the control volume from the lateral side, transporting ions away from the control volume to the adjacent control volumes. Thus, this leads to the expected conclusion that the ion mass fraction at the surface in the short-time regime is highly correlated with V_y right below the surface as illustrated in Fig. 6.

As a result, the ion mass fraction maxima at the surface for the short times correspond to the points of minimum velocity right beneath the surface. (We recall that the velocity is uniform right at the surface.)

It can also be noted that the number of local ion mass fraction local maxima (6) is the same as the number of permeability local minima. As we will see, this is different from the longer-time regime when the zone with significant ion mass gradients also develops in the region where the velocity field is highly correlated with the permeability.
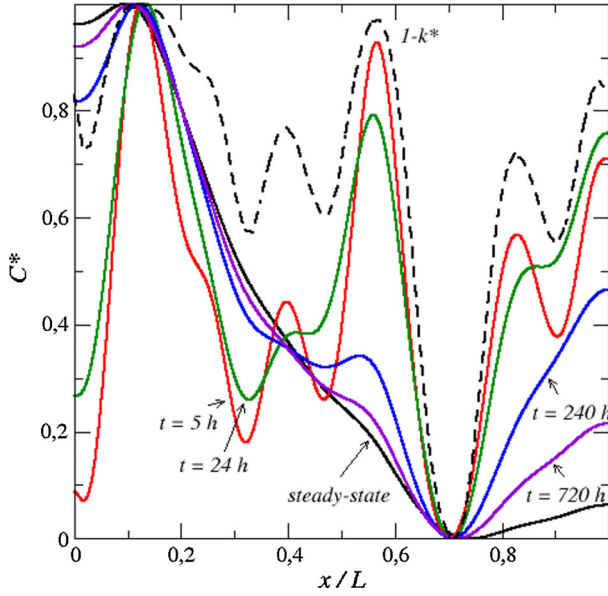
**Fig. 7** Variation of reduced concentration profiles at the surface as a function of time ($Pe \sim 6$)

However, it should be pointed out that the ion mass fraction depicted in Fig. 6 is in fact very weakly dependent on x, consistently with the fact that the velocity is uniform at the surface, i.e. in fact $C_{max} - C_{min}$ at $y = L$. Whereas the consideration of the reduced ion mass fraction C^* leads to the results shown in Fig. 6, it should be clear that other sources of variations, such as local variations in the evaporation flux at the surface or variations in the porosity (even tiny), would lead to other positions of the ion mass fraction maxima than indicated in Fig. 6, since in fact the ion mass fraction varies very little at the interface in the short-time regime when the variations are only due to the permeability disorder. As a result, starting with an initial salt mass fraction close to solubility is likely to lead to a different localization of crystallization spots than with a lower concentration owing to the sensitivity of the maxima positions to other factors than the permeability variations.

To investigate the impact of permeability variations, it is therefore more relevant to look at the distributions at longer times, where the amplitude of ion mass fraction variation at the surface can become quite important (when the Peclet number Pe is sufficiently high).

As exemplified in Fig. 7, the loci of ion fraction absolute maximum and absolute minimum at the surface are rapidly the same as the ones for the steady-state regime. For this reason, we only look at the steady-state ion distribution at the surface in what follows.

Since the ions cannot escape the system through the top and lateral boundaries, the average ion mass flux at the inlet is of course null when the steady state is reached. However, as illustrated in Fig. 8, the steady-state solution is characterized by a spatially non-uniform ion mass flux distribution over the inlet, consistently with the non-uniform velocity depicted in Fig. 3. As a result, the flux is positive in some sections of the inlet and negative elsewhere at the inlet. A positive flux means ions entering the system, while a negative flux means ions leaving the system at the inlet. As shown in Figs. 3 and 7, ions enter the system in the region of larger permeability where the velocity at the inlet is greater and leave the system in the region of lower permeability where the velocity is lower. In other terms, ions enter regions of

Fig. 8 Distribution of ion mass flux $\Phi(x, 0) = \varepsilon U_y C - \rho_\ell \varepsilon D_s^* \frac{\partial C}{\partial y}$ at the inlet in the steady-state regime for the reference case ($Pe \sim 6$)
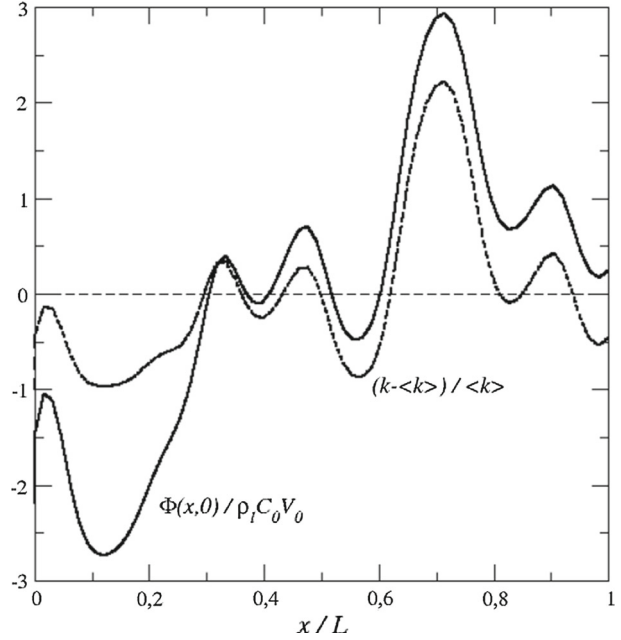
higher permeability, travel in those regions, then are redirected in the system towards regions of lower permeability where they travel back to the inlet where they exit.

Figure 9 shows the ion mass fraction distribution in the steady-state regime for various values of the Peclet number for the reference case. As can be seen, the ion mass fraction absolute maximum and minimum are well marked. (As indicated in the caption, the amplitude of the distribution is well marked in the long-time regime and increases with Peclet number.) The Peclet number is not a sensitive parameter as regards the loci of the two absolute extrema. The absolute maximum corresponds to the point of lowest permeability at the surface, whereas the point of highest permeability corresponds to the ion mass fraction absolute minimum at the interface. Thus, again, this is in contrast to the naïve examination of the velocity field depicted in Fig. 3, which would lead to the wrong conclusion that the maxima should correspond to the points of highest permeability.

The results shown in Fig. 9 suggest a simple rule. The ion concentration absolute maximum, i.e. the most likely place of crystallization, corresponds to the permeability absolute minimum and the ion concentration absolute minimum to the permeability absolute maximum.

To test this quite simple rule, we have generated a total of 10 realizations of the permeability random field and computed the steady-state solution for each realization for $Pe = 6$. Then, we have determined for each realization the positions at the surface of the permeability absolute minimum ($x_{k\text{min}}$) and absolute maximum ($x_{k\text{max}}$) as well as the positions at the surface of the ion mass fraction absolute minimum ($x_{C\text{min}}$) and absolute maximum ($x_{C\text{max}}$). Figure 10 shows the plots of the pairs ($x_{k\text{min}}$, $x_{C\text{max}}$) and ($x_{k\text{max}}$, $x_{C\text{min}}$) for the 10 realizations.

As can be seen, the tested rule is reasonable as regards the locus of the absolute ion mass maximum which corresponds reasonably well to the permeability absolute minimum for nine realizations out of the ten realizations. However, realization #2 is an exception with the position of the ion mass fraction absolute maximum clearly different from the position
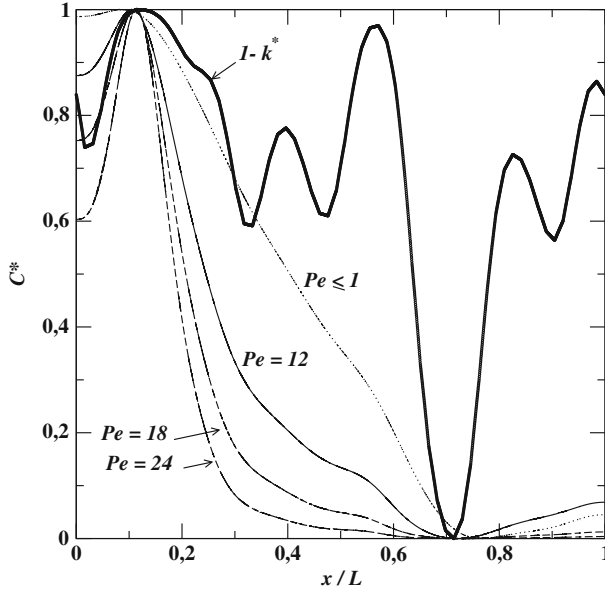
Fig. 9 Distribution of reduced ion mass fraction C^* at the porous medium surface for various Peclet number in the steady-state regime for the reference case. The amplitude ratio C_{max}/C_{min} is 1.06, 10, and 682 for Pe = 1.3, 12, and 24, respectively
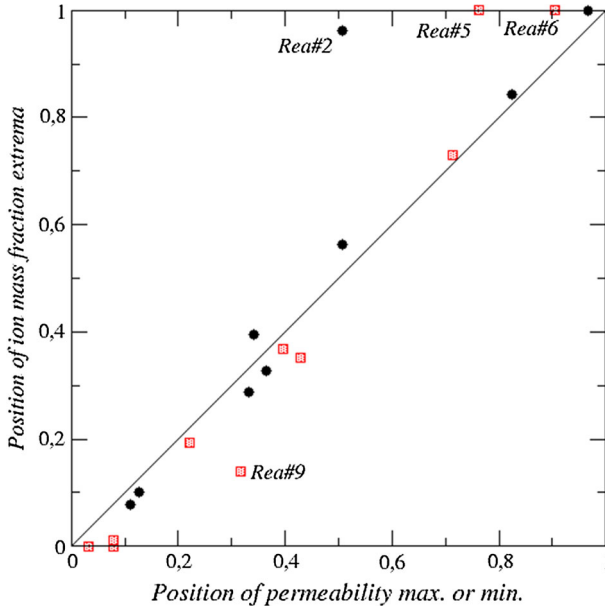

Fig. 10 Ion mass fraction absolute maximum position versus position of permeability absolute minimum at the surface (black filled circles). Ion mass fraction absolute minimum position versus position of permeability absolute maximum at the surface (red squares filled with dots). Results for 10 realizations

Fig. 11 Steady-state reduced permeability and ion mass fraction distributions at the surface for realization #2
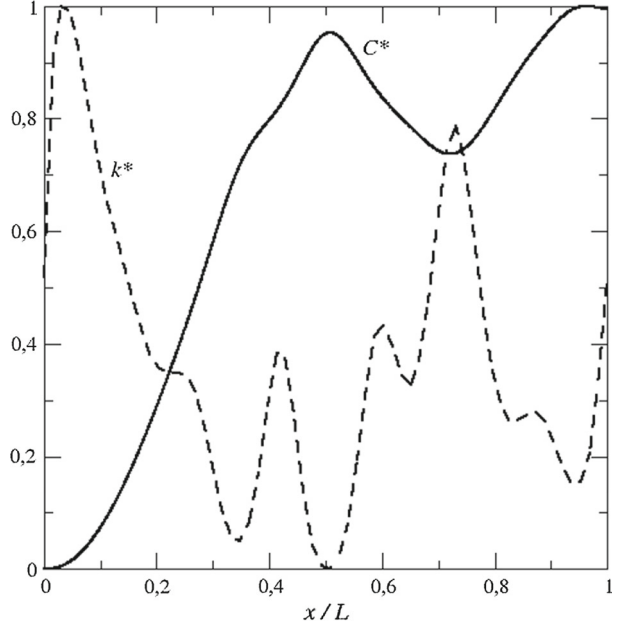
of the permeability absolute minimum. This is further illustrated in Fig. 11 showing the permeability and ion mass fraction distributions at the surface for this particular realization. As can be seen, the ion mass fraction corresponding to the locus of the permeability absolute minimum is actually quite close to the ion mass fraction absolute maximum but slightly lower. Also, it can be seen that the ion mass fraction absolute maximum corresponds to a local permeability minimum.

Figure 10 also indicates that the locus of the ion mass fraction minimum does not coincide with the locus of the permeability absolute maximum for three realizations.

A more detailed inspection of the results shows that an ion mass fraction local maximum corresponds to a permeability local minimum but not all permeability local minima correspond to an ion mass fraction local maximum. This is documented in Table 1. In spite of the quite low number of realizations, the trend is clear. The number of ion mass fraction local extrema is less than half the number of permeability local extrema (with $l_c/L \sim 1/12$ and considering that the distance between two minima (maxima, respectively) is on average on the order of two correlation lengths, the number of permeability minima (maxima, respectively) is expected to be on the order of $L/2l_c \sim 6$, which is consistent with the values reported in Table 1).

In order to explain this difference, we look in more details at the velocity field since the ion advection transport and thus the velocity field are key elements for the considered problem. More precisely, we look at the x-component of the velocity field at the surface since the velocity field is characterized by local redirection of the flow from greater permeability regions towards lower permeability regions in the top region of the system (Fig. 3). As illustrated in Fig. 12, this component at this position is on the same order of magnitude as the y-component, i.e. $\sim V_0$. Thus, there is a significant transversal advection transport near the surface. As exemplified in Fig. 12, this field is characterized by stagnation points, defined as the points where $V_x = 0$, at and in the vicinity of the surface. One can distinguish two

Table 1 Number of permeability local minima, permeability local maxima, ion mass fraction local maxima, ion mass fraction local minima, convergent stagnation points and divergent stagnation points

Realization	Permeability local minima	Ion mass fraction local maxima	Convergent stagnation points	Permeability local maxima	Ion mass fraction local minima	Divergent stagnation points
1	6	2	3	6	2	3
2	6	2	4	6	3	4
3	5	2	2	3	1	1
4	5	2	4	5	3	5
5	5	1	1	6	2	2
6	4	1	4	4	2	4
7	5	3	3	6	4	4
8	4	1	2	4	2	2
9	7	2	6	7	2	6
10	3	2	3	4	3	3
Averages over the 10 realizations	5	1.8	3.2	5.1	2.4	3.4

types of stagnation points: convergent stagnation points where the velocity on the right and the velocity on the left are directed towards the point, and divergent stagnation points where the velocities on the left and the right point outward from the considered point. Note that the point at $x = 0$ and $x = L$ is also considered as stagnation points since $V_x = 0$ at $x = 0$ and $x = L$. The convergent stagnation points correspond to local minima in the pressure field at the surface and the divergent stagnation points to pressure local maxima. There are three main convergent stagnation points in Fig. 12, at $x = 0$, at $x = L$ and the one indicated by arrows in Fig. 12 and one main divergent stagnation point (shown with arrows in Fig. 12). There are also one secondary convergent stagnation point and one secondary divergent point at $x \approx 0.5$ L. These two stagnation points are termed secondary because there are in a region of low transversal velocity and contrary to other stagnation points are not present anymore slightly further away from the surface, at $y = 0.95 L$ for example.

It is clear from Fig. 12 that a convergent stagnation point corresponds to a permeability local minimum and a divergent stagnation point to a permeability local maximum. However, as indicated in Table 1, the number of stagnation points at the surface is less than the number of permeability extrema. The ratio is about 2 (about twice less stagnation points than permeability local extrema) and thus closer to the number of ion mass fraction extrema. Actually, as shown in Fig. 13, the ion mass fraction absolute maxima (ion mass fraction absolute minima, respectively) do correspond to convergent stagnation points (divergent stagnation points, respectively). To make the plot depicted in Fig. 13, we have determined for each realization the positions at the surface of the ion mass fraction absolute maximum x_{Cmax} (absolute minimum x_{Cmin}, respectively) and then determined the position $x_{conv.st.p.}$ of the nearest convergent stagnation point ($x_{div.st.p}$ of nearest divergent stagnation point, respectively). Figure 13 shows the plots of the pairs $(x_{conv.st.p.}, x_{Cmax})$ and $(x_{div.st.p}, x_{Cmin})$ for the 10 realizations.
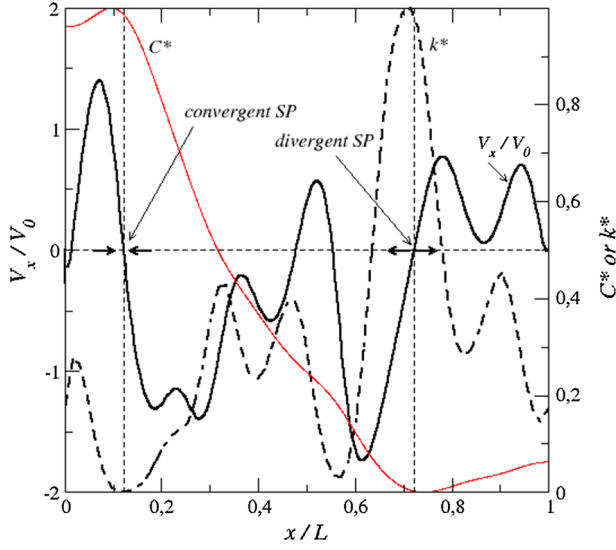
Fig. 12 Darcy's velocity component in x direction as a function of x at the surface. The distribution of reduced ion mass fraction C^* corresponds to the one shown in Fig. 7 for $Pe = 12$. SP stands for stagnation point
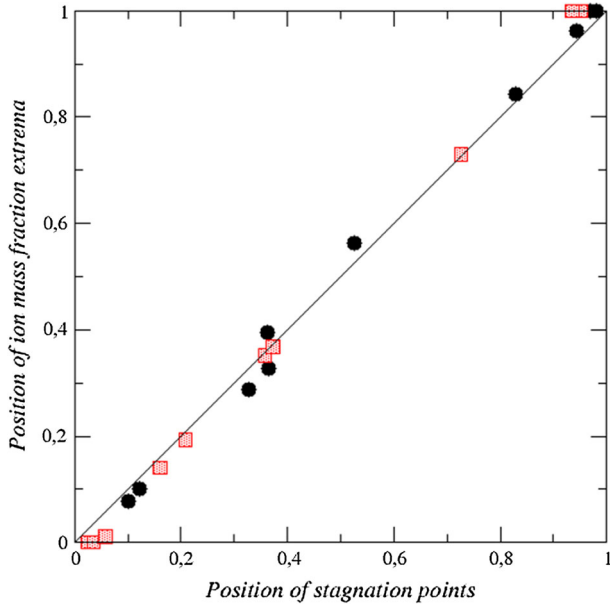

Fig. 13 Ion mass fraction absolute extrema position versus position of nearest stagnation point at the surface. Black filled circles correspond to ion mass fraction absolute maxima (and convergent stagnation points). Red squares with dots correspond to ion mass fraction absolute minima (and divergent stagnation points). Results for 10 realizations

7 Summary and Conclusions

We have explored numerically the impact of permeability heterogeneities on the ion concentration maxima at the evaporative surface of a porous medium in the evaporation–wicking situation assuming a spatially uniform evaporation flux at the surface.

Except at the very short times where the ion mass fraction is quasi-uniform at the surface, the ion mass fraction distribution at the surface does not present a simple relationship with the permeability distribution. The naïve view that would suggest that the number of ion mass fraction maxima should be on the order of $L/2l_c$ is wrong ($L/2l_c = 6$ in our simulations). In fact, the number of ion mass fraction maxima is about twice as much lower that the number of permeability local minima. Still more important, the situation is characterized by the formation of a well-marked absolute ion mass fraction maximum. In other terms, it is quite likely that only one crystallization spot forms at the surface with colonization of the surface from this spot.

The simulations indicate that the most likely place of the first crystal occurrence at the surface is the locus of the lowest permeability. This is somewhat counter-intuitive since the flow velocity is greater in the regions of greater permeability over most of the porous domain. However, the redirection of the flow towards the regions of lower permeability in the top region of the system eventually leads to the preferential formation of ion mass fraction maxima in the low permeability regions at the surface. However, it must be noted that the locus of the lowest permeability is not always the locus of the ion mass fraction absolute maximum. It can happen that the ion mass fraction absolute maximum forms at a different place corresponding to a permeability local minimum but different from the permeability absolute minimum.

It was also shown that the loci of the ion mass fraction extrema at the surface correspond to transversal velocity stagnation points with convergent stagnation points corresponding to ion mass fraction maxima and divergent stagnation points to ion mass fraction minima. However, no clear criterion was established to identify the ion mass fraction absolute maxima from properties of the stagnation points. For instance, the local slope of the velocity profile at the stagnation points does not allow ranking the stagnation points consistently with the locus of the ion mass fraction absolute extrema. (The ion mass fraction absolute maximum does not necessarily correspond to the convergent point of maximum slope.)

However, it should be emphasized that we have essentially explored the regime where the length $l_D = D_s^*/U_0$ is on the same order of magnitude as the permeability field transverse correlation length l_{cx}. The regime of higher Peclet numbers where $l_{cx} \gg l_D$ could be worth studying in relation to the findings reported in the present work.

As shown in Diouf et al. (2018) for the case of a simple system formed by the assembly of two vertical porous layers of different texture and in Hidri (2013) for random systems, the evaporation–wicking situation should be clearly distinguished from the drying situation when analysing the formation of crystals at the evaporative surface of a porous medium. Actually, the drying situation leads to opposed results compared to the evaporation–wicking situation (e.g. Diouf et al. 2018; Hidri 2013). Thus, it is expected that in drying the locus of first crystals corresponds to the permeability absolute maximum. This is so because of the preferential desaturation of the medium in the region of greater permeability. From a simple mass balance argument, the lower the local saturation decreases, the greater the ion local concentration increases since the dissolved salt cannot escape from the system. Although ions transport phenomena of course make the picture more complicated, it turns out that the

local increase in the ion concentration due to the local desaturation is often the dominant effect in drying as exemplified in Diouf et al. (2018).

Appendix

The filtration velocity distribution at the inlet of the system can be estimated as follows. Sufficiently away from the top surface the pressure only depends on z (thus is independent of x) and is the same in all media. Let us denote this pressure by P^*.

Thus, the velocity away from the evaporative surface can be expressed as

$$V_y = -\frac{k}{\mu}\frac{\mathrm{d}P^*}{\mathrm{d}y} \tag{A-1}$$

Since the velocity is known on the top surface ($V_y = V_0 = j/\rho_\ell$), expressing the flow rate conservation reads

$$\int_0^{L_x} V_y \mathrm{d}x = -\frac{1}{\mu}\frac{\mathrm{d}P^*}{\mathrm{d}y}\int_0^{L_x} k\mathrm{d}x = L_x V_0 \tag{A-2}$$

leading to

$$\frac{\mathrm{d}P^*}{\mathrm{d}z} = -\frac{\mu V_0}{\langle k \rangle} \tag{A-3}$$

where

$$\langle k \rangle = \frac{1}{L_x}\int_0^{L_x} k\mathrm{d}x \tag{A-4}$$

As a result, the velocity sufficiently away from the surface and thus at the inlet is given by

$$V_y = \frac{k}{\langle k \rangle} V_0 \tag{A-5}$$

References

Bear, J.: Dynamics of Fluids in Porous Media, vol. 1. American Elsevier Publishing Company (1972)

Bechtold, M., Haber-Pohlmeier, S., Vanderborght, J., Pohlmeier, A., Ferré, T.P.A., Vereecken, H.: Near-surface solute redistribution during evaporation. Geophys. Res. Lett. (2011). https://doi.org/10.1029/2011gl048147

Bergstad, M., Or, D., Withers, P.J., Shokri, N.: The influence of NaCl concentration on salt precipitation in heterogeneous porous media. Water Resour. Res. 53(2), 1702–1712 (2017). https://doi.org/10.1002/2016WR020060

Brutsaert, W.: Hydrology: An Introduction. Cambridge University Press, Cambridge (2005)

Dagan, G.: Flow and Transport in Porous Formations. Springer, Berlin (1989)

Dentz, M., Le Borgne, T., Englert, A., Bijeljic, B.: Mixing, spreading and reaction in heterogeneous media: a brief review. J. Contam. Hydrol. 120–121, 1–17 (2011). https://doi.org/10.1016/j.jconhyd.2010.05.002

Desarnaud, J., Derluyn, H., Molari, L., Miranda, S.D., Cnudde, V., Shahidzadeh, N.: Drying of salt contaminated porous media: effect of primary and secondary nucleation. J. Appl. Phys. 118(11), 114901 (2015). https://doi.org/10.1063/1.4930292

Diouf, B., Geoffroy, S., Abou-Chakra Guéry, A., Prat, M.: Locus of first crystals on the evaporative surface of a vertically textured porous medium. Eur. Phys. J. Appl. Phys. **81**(1), 11102 (2018)

Fried, J.J., Combarnous, M.A.: Dispersion in porous media. In: Chow, V.T. (ed.) Advances in Hydroscience, vol. 7, pp. 169–282. Elsevier, Amsterdam (1971)

Gelhar, L.W.: Stochastic Subsurface Hydrology. Prentice-Hall, Englewood Cliffs (1993)

Guglielmini, L., Gontcharov, A., Aldykiewicz Jr., A.J., Stone, H.A.: Drying of salt solutions in porous materials: Intermediate-time dynamics and efflorescence. Phys. Fluids **20**(7), 077101 (2008). https://doi.org/10.1063/1.2954037

Hidri, F.: Evaporation from a porous medium containing a dissolved salt. Influence of heterogeneities at Darcy's scale on the distribution of ions at the evaporative surface. Ph.D. Thesis (2013)

Hidri, F., Sghaier, N., Eloukabi, H., Prat, M., Nasrallah, S.B.: Porous medium coffee ring effect and other factors affecting the first crystallisation time of sodium chloride at the surface of a drying porous medium. Phys. Fluids **25**(12), 127101 (2013). https://doi.org/10.1063/1.4834356

Huinink, H.P., Pel, L., Michels, M.A.J.: How ions distribute in a drying porous medium: a simple model. Phys. Fluids **14**(4), 1389–1395 (2002). https://doi.org/10.1063/1.1451081

Kim, J.-H., Ochoa, J.A., Whitaker, S.: Diffusion in anisotropic porous media. Transp. Porous Media **2**(4), 327–356 (1987). https://doi.org/10.1007/BF00136440

Le Borgne, T., Dentz, M., Villermaux, E.: Stretching, Coalescence, and Mixing in Porous Media. Phys. Rev. Lett. **110**, 204501 (2013)

Mejri, E., Bouhlila, R., Helmig, R.: Heterogeneity effects on evaporation-induced halite and gypsum co-precipitation in porous media. Transp. Porous Media **118**(1), 39–64 (2017). https://doi.org/10.1007/s11242-017-0846-8

Nachshon, U., Shahraeeni, E., Or, D., Dragila, M., Weisbrod, N.: Infrared thermography of evaporative fluxes and dynamics of salt deposition on heterogeneous porous surfaces. Water Resour. Res. (2011a). https://doi.org/10.1029/2011wr010776

Nachshon, U., Weisbrod, N., Dragila, M.I., Grader, A.: Combined evaporation and salt precipitation in homogeneous and heterogeneous porous media. Water Resour. Res. (2011b). https://doi.org/10.1029/2010wr009677

Or, D., Lehmann, P., Shahraeeni, E., Shokri, N.: Advances in soil evaporation physics—a review. Vadose Zone J. (2013). https://doi.org/10.2136/vzj2012.0163

Penman, H.L.: Natural evaporation from open water, hare soil and grass. Proc. R. Soc. Lond. Ser. A Math. Phys. Sci. **193**(1032), 120–145 (1948)

Plouraboué, F., Flukiger, F., Prat, M., Crispel, P.: Geodesic network method for flows between two rough surfaces in contact. Phys. Rev. E **73**(3), 036305 (2006)

Puyate, Y.T., Lawrence, C.J.: Effect of solute parameters on wick action in concrete. Chem. Eng. Sci. **54**(19), 4257–4265 (1999). https://doi.org/10.1016/S0009-2509(99)00158-X

Puyate, Y.T., Lawrence, C.J.: Steady state solutions for chloride distribution due to wick action in concrete. Chem. Eng. Sci. **55**, 3329–3334 (2000). https://doi.org/10.1016/S0009-2509(99)00566-7

Puyate, Y.T., Lawrence, C.J., Buenfeld, N.R., McLoughlin, I.M.: Chloride transport models for wick action in concrete at large Peclet number. Phys. Fluids **10**(3), 566–575 (1998). https://doi.org/10.1063/1.869584

Slichter, C.S.: Field measurements of the rate of movement of underground waters. In: Water-Supply and Irrigation Paper No. 140, Series 0, Underground Waters, 43, Washington Government Printing Office (1905)

Veran-Tissoires, S., Prat, M.: Evaporation of a sodium chloride solution from a saturated porous medium with efflorescence formation. J. Fluid Mech. **749**, 701–749 (2014). https://doi.org/10.1017/jfm.2014.247

Veran-Tissoires, S., Marcoux, M., Prat, M.: Discrete salt crystallization at the surface of a porous medium. Phys. Rev. Lett. **108**(5), 054502 (2012a)

Veran-Tissoires, S., Marcoux, M., Prat, M.: Salt crystallisation at the surface of a heterogeneous porous medium. EPL (Europhys. Lett.) **98**(3), 34005 (2012b)